

---

# An Interpretable Baseline for Time Series Classification Without Intensive Learning

---

**Robert J. Ravier**

Department of ECE  
Duke University  
Durham, NC 27708  
robert.ravier@duke.edu

**Mohammadreza Soltani**

Department of ECE  
Duke University  
Durham, NC 27708  
mohammadreza.soltani@duke.edu

**Miguel Antunes Dias Alfaiate**

miguelalfaiatesimoes@gmail.com

**Denis Garagic**

BAE FAST Labs  
Burlington, MA 01803  
denis.garagic@baesystems.com

**Vahid Tarokh**

Department of ECE  
Duke University  
Durham, NC 27708  
vahid.tarokh@duke.edu

## Abstract

Recent advances in time series classification have largely focused on methods that either employ deep learning or utilize other machine learning models for feature extraction. Though such methods have proven powerful, they can also require computationally expensive models that may lack interpretability of results, or may require larger datasets than are freely available. In this paper, we propose an interpretable baseline based on representing each time series as a collection of probability distributions of extracted geometric features. The features used are intuitive and require minimal parameter tuning. We perform an exhaustive evaluation of our baseline on a large number of real datasets, showing that simple classifiers trained on these features exhibit surprising performance relative to state of the art methods requiring much more computational power. In particular, we show that our methodology achieves good performance on a challenging dataset involving the classification of fishing vessels, where our methods achieve good performance relative to the state of the art despite only having access to approximately two percent of the dataset used in training and evaluating this state of the art.

## 1 Introduction

Time series research has been an important focus of statistics for decades, thanks in large part due to the prevalence of time series in a wide number of fields such as finance [22, 32], medicine [37], illegal fishing [21, 7], among many others. Contemporary work has focused on utilizing increased computational abilities to move past ARIMA models [8] that heavily depend on certain assumptions that may not hold in practice.

The focus of this paper concerns time series classification. State of the art methods for this problem are largely ensemble methods [4, 3, 24, 29, 30]. These methods combine classical features, such as

dynamic time warping [5], with more modern features such as shapelets [38, 19] to develop classifiers that play off the successes and weaknesses of both the features and other simpler classifiers. These methods take a large amount of time and resources required to train and evaluate.

On the other hand, deep learning methods have been proposed as alternatives to ensemble models [9, 23, 34, 40, 25]. These methods seek to continue the widespread success that deep learning has seen in other applications. Many of these methods were analyzed in [16], where it was observed that some of them (in particular, ResNet [18]) performed extremely well relative to ensemble models. Further, the authors detailed experiments suggesting that deep learning models can focus their attention on certain regions of a time series in order to determine its classification. Though this study verified that deep learning models were making important contributions, the results still left things to be desired; their experiments required 60 GPUs, and the interpretability experiments only revealed the regions on *some* time series datasets that were of interest to *some* models, and does not reveal as to what feature was ultimately important in making a decision.

In the introduction of [16], the authors made an important point: the time series classification community had seemingly ignored the possibility that time series classification could be solved using pure feature learning algorithms. We take this question one step further: is it possible that well-studied, easy to compute mathematical features that could be used to train accurate, interpretable classifiers already exist? In this paper, we argue in the affirmative.

The goal of this work is to experimentally show that well-studied mathematical features can be used to build accurate and interpretable models. The main idea stems from the intuition that the trend (including any seasonality) of a time series contributes much more to its classification compared to any contribution observation noise may have. It has been independently observed on both trajectories [39, 13] and biological surfaces [27] that statistics of distributions of geometric features can create accurate classifiers. Though such features, known as interval features in the time series literature, have been proposed in the past [28, 11], we consider a set of features from differential geometry [12] that are important to the study of curves. By representing time series in terms of statistics of these distributions, we show extensive evidence that using these easy-to-compute features in tandem with either K-Nearest Neighbors (KNN) or Support Vector Machines (SVM) can perform competitively with state of the art deep learning models, even beating them in some cases. Our pipeline is easy to understand and readily adaptable to non-uniformly and asynchronously sampled time series. On univariate time series, we will see that KNN and SVM models trained on these features yield performance fairly close to the state of the art of deep learning, even beating it in a number of cases. In the multivariate setting, we will show that the combination of these features and models yields surprisingly good performance on trajectory classification in this setting despite having access to at most 2% of the data used by the state of the art [21].

The rest of the paper is outlined as follows. In Section 2, we discuss preliminaries and prior work related to our paper. In Section 3, we detail the general pipeline to obtain features and statistics needed we use for classification. In Section 4, we present results on both the aforementioned vessel classification problem as well as on the UCR/UEA time series archive used in [16, 10], showing the power of the proposed features we use. In Section 5, we discuss the role of certain parameters within the classification procedure. we make concluding remarks in Section 6. Additional experiments and details that do not fit within the page constraints of the main text will be deferred to the Appendix.

## 2 Preliminaries

### 2.1 Review

We begin with review and notation that we will use throughout the rest of the paper.

**Definition 1.** A  $d$ -dimensional time series is a sequence  $\mathbf{x} = x_{t_0}, \dots, x_{t_n} = \{x_{t_k}\}_{k=0}^n$ , where each  $x_{t_k}$  is a point in  $d$ -dimensional Euclidean space, and  $0 \leq t_k \leq T$ .

Note that we do not make the usual assumption that the  $t_k$  are equally spaced from one another, nor do we assume that all samples come from the same collection of times, as this is not true for some of our data. Nevertheless, we will require even spacing in time for our methods to work.

**Definition 2.** Let  $\mathbf{x} = \{x_{t_k}\}_{k=0}^n$  be a  $d$ -dimensional time series. Then we say that the function  $F_{\mathbf{x}}(t)$  defined for  $t_0 \leq t \leq t_n$  is the linear interpolant of  $\mathbf{x}$  if for  $t_i \leq t \leq t_{i+1}$ , we have

$$F_{\mathbf{x}}(t) = \frac{t - t_i}{t_{i+1} - t_i} x_{t_i} + \frac{t - t_{i+1}}{t_{i+1} - t_i} x_{t_{i+1}}. \quad (1)$$

Our use of linear interpolation is deliberate: it ensures that time series of physical quantities are still physically meaningful (e.g. interpolants of always positive quantities remain positive). By virtue of working with computers, we will never work directly with  $F_{\mathbf{x}}(t)$ , but rather with a discrete representation of it depending on our discretization of the interval  $[t_0, t_n]$ . Without further assumptions on  $\mathbf{x}$ , it is possible that  $F_{\mathbf{x}}$  may have sharp changes that make it unamenable to any analysis involving derivatives. To get around this, we require a smoothing operation.

**Definition 3.** Let  $f(u)$  be a function,  $a \leq u \leq b$ , taking values in  $d$ -dimensional space with a discrete representation given by  $(u_1, y_1), \dots, (u_N, y_N)$ . The Laplacian smoothing of the discrete representation is given by  $(u_1, \tilde{y}_1), \dots, (u_N, \tilde{y}_N)$ , where  $\tilde{y}_1 = y_1$ ,  $\tilde{y}_N = y_N$ , and for  $2 \leq k \leq N - 1$ ,

$$\tilde{y}_k = \frac{1}{2}(y_{k+1} - y_k) + \frac{1}{2}(y_{k-1} - y_k). \quad (2)$$

We will denote the first and second order derivatives of any function  $g$  of time by  $\dot{g}$  and  $\ddot{g}$ , respectively. All derivatives will be computed by usual first order approximations. We will use Definition 3 to smooth both functions and their derivatives in order to avoid numerical issues.

We also briefly review two classifiers of interest. For more information, see [17]. Given an embedding of a dataset into a metric space  $X$  with distance function  $\rho$ , a KNN classifier determines the label of a given data point  $z$  in the test by first determining the  $K$  closest points to  $z$  with respect to  $\rho$  in the training set, and then labeling  $z$  based on a function of the labels of the nearest neighbors. This function is generally either a majority vote, where the  $K$  nearest neighbors are either equally weighted or weighted such that points closer to  $z$  are given more influence. An SVM classifier seeks to learn a collection of separating hypersurfaces for datasets embedded in Euclidean space. Though SVM was originally a method to separate datapoints by means of separating hyperplanes, the kernel trick allows one to learn separating hypersurfaces via the use of a kernel function to define a new inner product; the hypersurfaces are hyperplanes with respect to this new inner product. Both methods are clearly interpretable, with decisions made based on geometric reasoning.

## 2.2 Related work

We briefly review the most relevant works to us and otherwise defer the reader to excellent review articles already published: see [1, 2, 16] for general overviews. Also, please see [26, 6] for trajectory methods.

Analogues of some the specific features we use in our method have been studied within the time series classification literature. In particular, a number of single-model classifiers of interest depend on the extraction of summary features of the behavior of a time series on a given subinterval, sometimes called interval features [28, 11]. One particular type of interval features of interest, shapelets, are subsequences of given time series that are chosen based on their perceived importance in determining the label of a given time series [38, 19]. Though interval features are natural to consider, they lead to a difficult question of determining which subintervals are most representative of a given class. This is a computationally expensive but necessary question in order to deal with both computational and memory limitations. We avoid these issues by using features that are determined locally around a given time sample, which neither requires a subinterval search nor an extensive amount of memory.

As stated in Section 1, the methodology used in [39, 13] is related to our work. Specifically, in [13], the authors extract a number of features from each time point sampled from a given trajectory. These features are then used to compile distributions of each feature that was observed over time. Next, these distributions are summarized by a number of statistics, including many of those we employ. The crucial difference in our work is the simultaneous increase the mathematical rigor of their treatment of bearing (the direction in which a trajectory is moving), which is incompatible with quantities of interest from differential geometry. Moreover, our approach is generalizable and applicable to more

general time series for which the analogous information is not immediately given. Finally, we propose the use of additional statistical quantities of interest, which based on our presented experiments have nontrivial roles in establishing the accuracy of a classifier.

### 3 Representing Time Series by Statistics of Distributions

#### 3.1 Velocity, curvature, and their importance in determining trends

As previously stated, our methodology is based on intuition that the trend of a time series is of much greater importance than any observed noise. Thus, for this subsection, we assume that  $\mathbf{x}$  is a smoothly varying time series such that the time between samples is small (we can always obtain such a time series from an initial through a combination of linear interpolation and Laplacian smoothing). The assumption that  $\mathbf{x}$  is smoothly varying is not restrictive as it is well-known that differentiable functions can well-approximate continuous functions

A  $d$ -dimensional time series  $\mathbf{x}$  can be regarded as a sample of a curve in  $d + 1$ -dimensional space: the coordinates at time  $t$  of such a curve are  $(t, \mathbf{x}_t)$ . The velocity of a curve is given by

$$\mathbf{v} := (1, \dot{\mathbf{x}}),$$

and its value at any one point in time uniquely determines the curve; this is a consequence of the fundamental theorem of calculus. It is thus natural that the values of the time series and its derivatives are needed for any interpretable classifier. There is another feature of critical interest: *curvature*.

**Definition 4.** The curvature vector of a  $d$ -dimensional time series  $\mathbf{x}$  is given by  $\kappa(\mathbf{x}) := \hat{\mathbf{v}}_{\mathbf{n}}$ , where

$$\mathbf{v}_{\mathbf{n}} := \frac{\mathbf{v}}{\|\mathbf{v}\|}, \quad (3)$$

where  $\|\cdot\|$  is the Euclidean norm. As both the name and definition imply, curvature attempts to quantify the change of the direction in which a curve is moving that is independent of magnitude of the velocity. The curvature vector is of utmost importance in the study of curves in differential geometry: it is a key component of a *Darboux frame*, which is known to uniquely determine a smooth curve up to Euclidean motion [31]. The full power of Darboux frames are well out of scope of this work, though are of great importance and interest in studying the classification of time series on non-Euclidean spaces, which we leave for future work. It is important to note, however that planar curves (e.g. univariate time series) are fully determined by their curvature vector [12]. Thus, curvature vectors are also important features to employ.

For this work, we limit ourselves to  $\|\kappa(\mathbf{x})\|$ , known simply as *curvature*. Our choice is again motivated by intuition: it is the sharpness of a curve rather than a specific direction that matters more. For univariate time series, it is easily derived that

$$\|\kappa(\mathbf{x})\| = \frac{|\ddot{\mathbf{x}}|}{\|1 + \dot{\mathbf{x}}^2\|^{3/2}}. \quad (4)$$

Given this, we also use the *signed curvature*, obtained by removing the absolute value in the numerator of Equation 4. The added sign gives information as to the nature of how the time series changes that would not be present otherwise.

#### 3.2 Distribution extraction methodology

For a given possibly non-uniformly sampled time series  $\mathbf{x}$ , we follow the below pipeline for extracting distributions from which we derive features.

1. Upsample  $\mathbf{x}$  if necessary using linear interpolation to reach the desired resolution of points
2. Apply the desired number of iterations of Laplacian smoothing in Definition 3, compute  $\dot{\mathbf{x}}$ , and apply the same number of iterations of Laplacian smoothing to  $\dot{\mathbf{x}}$ .
3. Compute  $\ddot{\mathbf{x}}$ ,  $\|\ddot{\mathbf{x}}\|$ , and  $\|\kappa(\mathbf{x})\|$ , and apply Laplacian smoothing.
4. Extract empirical distributions of relevant features:

- For univariate time series:  $\mathbf{x}$ ,  $\dot{\mathbf{x}}$ ,  $\ddot{\mathbf{x}}$ , the curvature, and the signed curvature.
- For multivariate time series:  $\mathbf{x}$ ,  $\|\dot{\mathbf{x}}\|$ , the derivative of  $\|\dot{\mathbf{x}}\|$ ,

and other potentially relevant problem-dependent information, where each sample in the empirical distributions is the value of the corresponding feature at each point in time.

### 3.3 Determining the feature representation

For real-valued distributions, we use the following standard statistics: range, mean, standard deviation, skew, kurtosis, and quantiles. This differs from those used in [13] in a number of ways. Here, we choose to extract skew and kurtosis in order to capture different notions of spread that are not well captured by the other features. In addition, we will also use a more extensive set of quantiles, notably a larger number of quantiles towards the tails of each distribution so as to better capture extremal behavior.

For multivariate time series, position is not properly real-valued. Because of this, the resulting statistics that we can reasonably take are limited; quantiles, for example, do not make sense as there is no natural order to Euclidean space. We instead derive statistics based off of the following quantity:

$$\sigma^2(p) = \sum_{i=1}^n d^2(p_i, p), \quad (5)$$

where the  $p_i$  are points on the sphere and  $d^2(\cdot, \cdot)$  is the squared distance between two points on the sphere. The minimum of this function is known as the *Frechet variance*, and any  $p$  that attains this minimum is known as a *Frechet mean*. For Euclidean space, this is the same as the usual mean; this quantity is, however, useful for spherical-valued and other non-Euclidean valued time series. Note that though the Frechet mean is in general not unique, it is if the  $p_i$  in the summation are within a small enough neighborhood on the sphere [20]. In practice, it is easy to compute both quantities by brute force, and we did not run into any issues of nonuniqueness for the data considered. Note that the Frechet variance is always meaningful in general, even if the Frechet mean is not unique.

### 3.4 Representation by features on windows

The statistics from the last section are determined by values over the entire series. Though the representation constructed is meaningful, it has been observed in [16] that modern deep learning classifiers may learn local features in order to make accurate predictions. Such locality cannot be properly observed using the representation described above. Nevertheless, it is easy to develop a meaningful representation of each time series: divide the time series into windows of equal size, compute the relevant statistics in each window, and represent the entire time series as a concatenation of all of the features. This naturally increases the resolution of information.

## 4 Evaluation and Comparison

### 4.1 Comparison on the univariate UCR/UEA archive

In order to evaluate the capabilities of combining the aforementioned features with interpretable classifiers, we compare the results of KNN and SVM classifiers trained on these features with recent deep learning classifiers analyzed in [16]. Specifically, we compare our trained interpretable classifiers to these models on the UCR/UEA time series repository [10], a collection of 85 univariate time series datasets used to evaluate the performance of classifiers, with each dataset having its own fixed sets for training and test. We follow the convention of [16] and measure the performance of each classifier by the mean accuracy averaged over ten experiments.

For each classifier, we test the performance based on four separate collections of features. In addition to representing each time series by the global statistics from the previous section mentioned, we also follow the last part of Section 3 and represent each time series as a concatenation of the above statistics obtained on disjoint windows of equal size. Specifically, we divide each time series into 2, 4, and 6 windows of equal length, compute the statistics on each of the 2, 4, and 6 windows respectively, and represent each time series as a concatenation of the statistics on the 2, 4, and 6 windows respectively. The idea is to allow some local information to be fed into the classifier, which

Table 1: Average accuracy of KNN and SVM with our proposed features relative to the top 3 deep learning architectures (per dataset) from [16] for the 15 largest and 15 smallest datasets from the UCR/UEA archive.

Dataset	Top1	Top2	Top3	DIST_KNN	DIST_KNN_2	DIST_KNN_4	DIST_KNN_6	DIST_SVM	DIST_SVM_2	DIST_SVM_4	DIST_SVM_6
ChlorineConcentration	<b>0.8436</b>	0.8138	0.8020	0.5982	0.6573	0.6948	0.4669	0.6060	0.6591	0.7029	0.5326
ECG5000	0.9401	0.9398	0.9368	0.9348	0.9408	0.9365	0.9437	0.9362	0.9106	0.9338	<b>0.9466</b>
ElectricDevices	<b>0.7291</b>	0.7019	0.6813	0.5384	0.5778	0.5844	0.6019	0.5055	0.6078	0.6043	0.6094
FordA	<b>0.9234</b>	0.9205	0.9036	0.7592	0.7605	0.7631	0.7588	0.8265	0.8188	0.8318	0.8402
NonInvasiveFatalECG_Thorax1	<b>0.9564</b>	0.9454	0.9156	0.8195	0.8397	0.8472	0.8434	0.8960	0.9059	0.9213	0.9107
NonInvasiveFatalECG_Thorax2	<b>0.9532</b>	0.9461	0.9316	0.8276	0.8418	0.8521	0.8418	0.8826	0.8941	0.8959	0.8921
StarLightCurves	0.9718	0.9614	0.9569	0.9760	0.9731	0.9748	0.9713	0.9779	<b>0.9785</b>	0.9771	0.9771
Two_Patterns	<b>1.0000</b>	0.9997	0.9461	0.7083	0.7873	0.7503	0.8300	0.7680	0.9245	0.9705	0.9565
UWaveGestureLibraryAll	0.9545	0.7860	0.7805	0.6573	0.8619	0.9226	0.9459	0.7357	0.9040	0.9497	<b>0.9563</b>
uWaveGestureLibrary_X	0.7671	0.6962	0.6701	0.6900	0.7695	0.8034	0.8010	0.7321	0.8088	<b>0.8118</b>	0.8046
uWaveGestureLibrary_Y	<b>0.7501</b>	0.7263	0.7115	0.6165	0.7041	0.7340	0.7315	0.6415	0.7418	0.7496	0.7415
uWaveGestureLibrary_Z	<b>0.9543</b>	0.9285	0.9178	0.6222	0.7073	0.7379	0.7356	0.6803	0.7370	0.7487	0.7429
wafer	<b>0.9986</b>	0.9971	0.9964	0.9942	0.9940	0.9955	0.9966	0.9961	0.9951	0.9932	0.9826
yoga	<b>0.8702</b>	0.8547	0.8385	0.7864	0.8047	0.8331	0.8295	0.8093	0.8233	0.8523	0.8393
PhalangesOutlinesCorrect	<b>0.8390</b>	0.8202	0.8033	0.7107	0.7221	0.7147	0.7272	0.7576	0.7494	0.7669	0.7739
Beef	0.7633	0.7533	0.7200	0.5667	0.5933	0.6200	<b>1.0000</b>	0.6267	0.7467	0.8000	<b>1.0000</b>
BeetleFly	0.8900	0.8700	0.8600	0.8500	0.8550	0.8950	<b>1.0000</b>	0.8900	0.7000	0.8400	<b>1.0000</b>
BirdChicken	0.9550	0.8850	0.7750	0.9000	0.9000	0.9000	<b>1.0000</b>	0.9000	0.9000	0.9000	<b>1.0000</b>
Car	0.9250	0.9050	0.7833	0.6900	0.7983	0.7400	0.1833	0.7167	<b>0.9811</b>	0.9700	0.4954
Coffee	<b>1.0000</b>	<b>1.0000</b>	0.9964	0.9643	0.9357	0.9643	0.9571	0.9643	<b>1.0000</b>	<b>1.0000</b>	0.9643
FaceFour	<b>0.9545</b>	0.9284	0.9057	0.6591	0.5625	0.5795	0.6920	0.7159	0.5636	0.5682	0.7614
Herring	0.6188	0.6078	0.6000	0.5031	0.4969	0.5266	0.5781	<b>0.6594</b>	0.6578	0.6359	0.6234
Lighting2	0.7705	0.7393	0.7033	0.7689	0.7492	0.8033	0.8066	<b>0.8115</b>	0.7508	0.7557	0.7098
Lighting7	<b>0.8452</b>	0.8274	0.6644	0.6055	0.6945	0.7384	0.7589	0.7151	0.7397	0.7644	0.7315
Meat	0.9683	0.9683	0.9017	0.8833	0.9333	0.9533	0.9250	0.9667	0.9500	<b>0.9833</b>	0.9500
OliveOil	0.8300	0.7900	0.7233	0.8333	0.8300	<b>0.8833</b>	0.8567	0.8667	0.8488	0.8099	0.8595
ShapeletSim	0.7794	0.7244	0.6167	0.9172	0.7856	0.7222	0.6889	<b>0.9694</b>	0.9111	0.7661	0.7128
ToeSegmentation2	<b>0.9062</b>	0.8800	0.8423	0.7100	0.6238	0.7515	0.7738	0.6231	0.6538	0.6308	0.7792
Trace	<b>1.0000</b>	<b>1.0000</b>	0.9600	0.9180	<b>1.0000</b>	0.9900	0.9500	0.9800	<b>1.0000</b>	0.9900	0.9900
Wine	0.7593	0.7444	0.5870	0.5778	0.5556	0.5759	0.5333	0.5556	<b>0.8333</b>	0.7074	0.7074

Table 2: Number of times a given model and feature combination achieves a given rank relative to seven top deep learning models in [16].

Model	1st	2nd	3rd	4th	5th	6th	7th	8th
1-Window KNN	6	2	14	6	10	13	16	18
2-Window KNN	8	5	17	12	11	12	11	9
4-Window KNN	8	6	19	12	10	11	10	9
6-Window KNN	12	5	17	8	6	11	11	15
1-Window SVM	9	6	21	9	11	8	11	10
2-Window SVM	12	11	25	9	8	8	7	5
4-Window SVM	14	13	22	12	11	3	6	4
6-Window SVM	18	3	24	7	9	6	5	13
Best KNN	15	6	24	9	9	8	9	5
Best SVM	28	6	29	8	4	4	4	2

would potentially not be easily distinguishable if no such division took place. These models are listed as DIST\_KNN\_ $n$  and DIST\_SVM\_ $n$ , where  $n$  is the number of windows used, respectively.

#### 4.1.1 Experimental setup

Each time series was linearly interpolated, if necessary, to be 500 equally spaced time samples. One iteration of Laplacian smoothing was applied for each derivative taken. Each KNN and SVM classifier was trained using 10-fold cross validation on the given training set; hyperparameters and settings are given in the Appendix. Feature extraction was performed in Python3 using SciPy on a Windows 10 Laptop with a 2.2GHz i7-8750H CPU with 16 GB of RAM. Classification results for KNN and SVM models were obtained using Python3 and SciPy packages on an Ubuntu cluster with four 2.1 GHz Xeon Gold 6152 CPUs and 360 GB of RAM [33]. We compare our results to those in [16].

#### 4.1.2 Performance

In Table 1, we compare each KNN and SVM model trained with the top 3 models per dataset (Top1, Top2, Top3) of seven models taken from [16] on thirty of the UCR/UEA univariate datasets. The datasets chosen are the fifteen largest and the fifteen smallest. The remaining results are in the supplementary material. We left out both Time-CNN and t-LeNet due to their poor performance when analyzed in [16]. The KNN and SVM models generally outperform deep learning models on the least populous datasets, and achieve perfect performance in some cases (e.g. Beef, BeetleFly, and

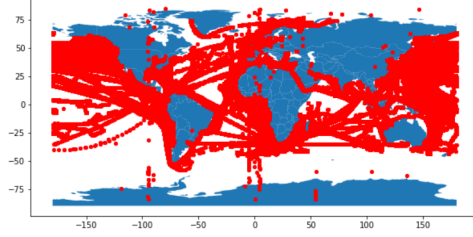


Figure 1: Spatial range of one hundred vessels in the Global Fishing Watch dataset [36]. Red indicates a coordinate reached by one of the vessels.

Table 3: Statistics of 10-fold nested cross validation scores for KNN and SVM with respect to the given features.

Model	Min	Max	Mean	Std
KNN	0.654898	0.688304668	0.670104832	0.007904
SVM	0.681032	0.702760033	0.692059241	0.006092

BirdChicken). Deep learning generally performs better on larger datasets; although, the best of the KNN and SVM models is often competitive and state of the art in some.

In Table 2, we list the relative performance rank of each of the eight classifiers we considered relative to the seven deep learning models considered for each of the 85 datasets. Of particular interest is that 2-Window, 4-Window, and 6-Window SVM, when individually compared with the other seven deep learning models, are within the top 3 for *over half* of the datasets evaluated on. In addition, the best performing SVM model (per dataset) is better than all but at most two of the deep learning models for 74.1% of the datasets considered; similarly, the best performing KNN model per dataset is better than all but at most two of the deep learning models for 52.9% of the datasets, suggesting that the explicit features we employed are potentially capturing a large amount of information that the top deep learning models are capturing. Further experimental results on the UCR 2018 dataset (featuring 128 time series, including the previous 85) that support this are detailed in the Appendix.

## 4.2 Multivariate Case Study: Vessel Classification

As previously mentioned in Section 1, we will evaluate the performance of our method in the multivariate setting on a challenging dataset from Global Fishing Watch [36, 35]. This dataset consists of 1258 vessel trajectories spanning the entire globe (a sphere) over a period of four years. Figure 4.2 shows the spatial range of one hundred of these trajectories (with some GPS errors) over this time period. Of these, 1107 are labeled with one of twelve different vessel classes. The goal is accurate classification. The current state of the art on this problem given in [21] is a large CNN that was trained and tested on a much larger superset of the data freely available; we have approximately 2% of what was used. Their model achieves a high classification accuracy of approximately 95% on a fixed training set of 52,964 and a test set of 22,172. We are interested in seeing if the features employed combined with SVM and KNN models can yield good performance despite a lack of data. Note that this dataset requires a fair amount of preprocessing before we use it; details are given in the Appendix. In particular, irregular sampling rates are relevant to vessel behavior [21].

Given the geographic scope of the data, the dataset that we have to work with is itself relatively small. We ideally need access to as much data as possible, but formally holding out a fixed dataset would perhaps highly bias our result. We instead use 10-fold *nested cross-validation*, which allows us to generate random train-validation-test splits. To be more precise, we will first split the dataset into 10 parts of equal size. One of these parts will act as a holdout set. The other nine parts will be combined and then split into another 10 pieces, which we will run cross-validation on to tune hyperparameters (the same as in the previous section). Based on these chosen hyperparameters, the final loss is evaluated on the holdout set from the first split. This is repeated so that each of the folds is used as a holdout set; the final loss is the average of the losses for each holdout set.

We performed thirty iterations of this 10-fold nested cross validation procedure. Statistics of these thirty iterations are given in Table 3. Both models perform surprisingly well in this scenario, with KNN and SVM achieving 67% and 69% accuracy on average, respectively, whereas approximately 50-times as much data with a deep learning model achieves 95% accuracy for a fixed train and test split. We give a confusion matrix in the Appendix for a fixed nested cross-validation iteration. In particular, note that a large amount of the accuracy comes from confusing certain classes of vessels, such as reefers and cargo/tankers, which have similar movement patterns and are thus potentially mistakable by just trajectory information alone.

## 5 Empirical Studies

In the following, we summarize a number of experiments concerning various parameters used in our methods. Full details for all of these are given in the Appendix.

### 5.1 Amount of Laplacian smoothings

We tested the effect of the amount of smoothing we employed on each of the UCR/UEA datasets. In particular, we also reran our experiments using both zero iterations of smoothing per derivative and two iterations. The particular effect on performance was dataset-dependent. In particular, smoothing both notably increased and decreased accuracy depending on the dataset. This suggests that any choice of amount of smoothing should be dataset dependent and not fixed for every possible dataset.

### 5.2 Parameter ablation studies

We tested the role of different features on the GFW dataset. Specifically, we tested the effect of removing specific geometric features (e.g. position, curvature) and specific statistics on classifier performance. Both KNN and SVM were negatively affected by the removal of non-tail quantiles, position, and speed information. SVM was negatively affected by the removal of all acceleration and curvature information, as well as the removal of some information concerning irregularity of sampling. KNN, on the other hand, seemed to improve in performance with the acceleration and curvature information removed. However, given the generally superior performance of SVM, this leads us to believe that the second derivative information plays a significant positive role in improving accuracy.

### 5.3 Effect of specific windows

As discussed in [16], some of the previous success of deep learning on time series classification might be attributed to the ability to learn localized features; the performance of KNN and SVM with multiple windows suggests the same. To test this, we trained both KNN and SVM classifiers on the statistics from each of the individual windows extracted on the 6-window dataset. Though restricting to individual windows does not appear to improve performance, near-perfect or perfect classification results can be achieved using only information from specific windows (e.g. Beef, BeetleFly, Bird-Chicken, and StarlightCurves). This suggests that future improvements on classification success may rely on the ability for a model to find local areas of interest, at least in certain cases. Other results show (e.g. on the Adiac and Cricket datasets), however, that this is not true in general.

## 6 Conclusion

In this paper, we showed that explicit features, namely statistics of known geometric features, can be used to train accurate interpretable time series classifiers. We showed that this particular combination yields classifiers that are exceptionally competitive with deep learning methods, achieving state of the art performance on a number of real datasets. We also showed that such methods achieve good performance on the difficult, limited multivariate Global Fishing Watch dataset relative to that of the state of the art despite the small amount of data available.

Given the simplicity of this construction, we believe that both the features presented and variants of the models discussed will be very important to understanding time series classification. Specifically, since our methods were competitive with deep learning, we believe this may lead to insight as to



what deep learning methods may detect in their classification procedure, as well as more accurate general classifiers.

## 7 Acknowledgements

This work was supported in part by DARPA Grant No. HR00111990016.

## Broader Impact

As time series is a topic with a wide variety of applications outside of machine learning, we believe that practitioners who utilize time series may find the insights enlightening, and will perhaps provide language (namely surrounding curvature, which to the best of our knowledge has not been widely discussed within the time series community) that will capture concepts that they (the practitioners) have investigated for a while. It may also help shed light on other black boxes researchers have been using, at least as a potential explanation for what may be occurring within said black box. However, since time series is a topic of wide interest, it is possible that some may use this work for nefarious purposes, but we do not immediately recognize what such purposes may be.

To the best of our knowledge, the only consequence of failure is incorrect classification, which may or may not be harmful depending on the circumstance. The success of the classifier is inevitably biased to what it was trained on, but that is no different than other methods used.

## References

- [1] S. Aghabozorgi, A. S. Shirkhorshidi, and T. Y. Wah. Time-series clustering—a decade review. *Information Systems*, 53:16–38, 2015.
- [2] A. Bagnall, J. Lines, A. Bostrom, J. Large, and E. Keogh. The great time series classification bake off: a review and experimental evaluation of recent algorithmic advances. *Data Mining and Knowledge Discovery*, 31(3):606–660, 2017.
- [3] A. Bagnall, J. Lines, J. Hills, and A. Bostrom. Time-series classification with cote: the collective of transformation-based ensembles. *IEEE Transactions on Knowledge and Data Engineering*, 27(9):2522–2535, 2015.
- [4] M. G. Baydogan, G. Runger, and E. Tuv. A bag-of-features framework to classify time series. *IEEE transactions on pattern analysis and machine intelligence*, 35(11):2796–2802, 2013.
- [5] D. J. Berndt and J. Clifford. Using dynamic time warping to find patterns in time series. In *KDD workshop*, volume 10, pages 359–370. Seattle, WA, 1994.
- [6] J. Bian, D. Tian, Y. Tang, and D. Tao. Trajectory data classification: A review. *ACM Transactions on Intelligent Systems and Technology (TIST)*, 10(4):1–34, 2019.
- [7] K. Boerder, N. A. Miller, and B. Worm. Global hot spots of transshipment of fish catch at sea. *Science advances*, 4(7):eaat7159, 2018.
- [8] G. E. Box, G. M. Jenkins, G. C. Reinsel, and G. M. Ljung. *Time series analysis: forecasting and control*. John Wiley & Sons, 2015.
- [9] Z. Cui, W. Chen, and Y. Chen. Multi-scale convolutional neural networks for time series classification. *arXiv preprint arXiv:1603.06995*, 2016.
- [10] H. A. Dau, A. Bagnall, K. Kamgar, C.-C. M. Yeh, Y. Zhu, S. Gharghabi, C. A. Ratanamahatana, and E. Keogh. The ucr time series archive. *IEEE/CAA Journal of Automatica Sinica*, 6(6):1293–1305, 2019.
- [11] H. Deng, G. Runger, E. Tuv, and M. Vladimir. A time series forest for classification and feature extraction. *Information Sciences*, 239:142–153, 2013.
- [12] M. P. Do Carmo. *Differential geometry of curves and surfaces: revised and updated second edition*. Courier Dover Publications, 2016.
- [13] M. Etemad, A. S. Júnior, and S. Matwin. Predicting transportation modes of gps trajectories using feature engineering and noise removal. In *Canadian conference on artificial intelligence*, pages 259–264. Springer, 2018.

- [14] H. Fawaz. Deep learning for time series classification. <https://github.com/hfawaz/dl-4-tsc>, 2019.
- [15] H. Fawaz. Ucr time series classification archive. [https://www.cs.ucr.edu/~eamonn/time\\_series\\_data\\_2018/](https://www.cs.ucr.edu/~eamonn/time_series_data_2018/), 2019.
- [16] H. I. Fawaz, G. Forestier, J. Weber, L. Idoumghar, and P.-A. Muller. Deep learning for time series classification: a review. *Data Mining and Knowledge Discovery*, 33(4):917–963, 2019.
- [17] T. Hastie, R. Tibshirani, and J. Friedman. *The elements of statistical learning: data mining, inference, and prediction*. Springer Science & Business Media, 2009.
- [18] K. He, X. Zhang, S. Ren, and J. Sun. Deep residual learning for image recognition. In *Proceedings of the IEEE conference on computer vision and pattern recognition*, pages 770–778, 2016.
- [19] J. Hills, J. Lines, E. Baranauskas, J. Mapp, and A. Bagnall. Classification of time series by shapelet transformation. *Data Mining and Knowledge Discovery*, 28(4):851–881, 2014.
- [20] H. Karcher. Riemannian center of mass and mollifier smoothing. *Communications on pure and applied mathematics*, 30(5):509–541, 1977.
- [21] D. A. Kroodsma, J. Mayorga, T. Hochberg, N. A. Miller, K. Boerder, F. Ferretti, A. Wilson, B. Bergman, T. D. White, B. A. Block, et al. Tracking the global footprint of fisheries. *Science*, 359(6378):904–908, 2018.
- [22] M. Kumar, N. R. Patel, and J. Woo. Clustering seasonality patterns in the presence of errors. In *Proceedings of the eighth ACM SIGKDD international conference on Knowledge discovery and data mining*, pages 557–563, 2002.
- [23] A. Le Guennec, S. Malinowski, and R. Tavenard. Data augmentation for time series classification using convolutional neural networks. In *ECML/PKDD Workshop on Advanced Analytics and Learning on Temporal Data*, 2016.
- [24] J. Lines, S. Taylor, and A. Bagnall. Hive-cote: The hierarchical vote collective of transformation-based ensembles for time series classification. In *2016 IEEE 16th international conference on data mining (ICDM)*, pages 1041–1046. IEEE, 2016.
- [25] Q. Ma, J. Zheng, S. Li, and G. W. Cottrell. Learning representations for time series clustering. In *Advances in Neural Information Processing Systems*, pages 3776–3786, 2019.
- [26] J. D. Mazimpaka and S. Timpf. Trajectory data mining: A review of methods and applications. *Journal of Spatial Information Science*, 2016(13):61–99, 2016.
- [27] R. Ravier, H. Kirveslahti, D. Boyer, and I. Daubechies. A new correspondence-free metric for anatomical surfaces. In *preparation*, 2020.
- [28] J. J. Rodríguez and C. J. Alonso. Support vector machines of interval-based features for time series classification. In *International Conference on Innovative Techniques and Applications of Artificial Intelligence*, pages 244–257. Springer, 2004.
- [29] P. Schäfer and U. Leser. Fast and accurate time series classification with weasel. In *Proceedings of the 2017 ACM on Conference on Information and Knowledge Management*, pages 637–646, 2017.
- [30] A. Shifaz, C. Pelletier, F. Petitjean, and G. I. Webb. Ts-chief: A scalable and accurate forest algorithm for time series classification. *Data Mining and Knowledge Discovery*, pages 1–34, 2020.
- [31] M. D. Spivak. *A comprehensive introduction to differential geometry*. Publish or perish, 1970.
- [32] S. J. Taylor. *Modelling financial time series*. world scientific, 2008.
- [33] P. Virtanen, R. Gommers, T. E. Oliphant, M. Haberland, T. Reddy, D. Cournapeau, E. Burovski, P. Peterson, W. Weckesser, J. Bright, et al. Scipy 1.0: fundamental algorithms for scientific computing in python. *Nature Methods*, pages 1–12, 2020.
- [34] Z. Wang, W. Yan, and T. Oates. Time series classification from scratch with deep neural networks: A strong baseline. In *2017 International joint conference on neural networks (IJCNN)*, pages 1578–1585. IEEE, 2017.
- [35] G. F. Watch. Datasets and code. <https://globalfishingwatch.org/datasets-and-code/ais-and-other-data/>, 2017.

- [36] G. F. Watch. Training data. <https://github.com/GlobalFishingWatch/training-data>, 2017.
- [37] A. Wismüller, O. Lange, D. R. Dersch, G. L. Leinsinger, K. Hahn, B. Pütz, and D. Auer. Cluster analysis of biomedical image time-series. *International Journal of Computer Vision*, 46(2):103–128, 2002.
- [38] L. Ye and E. Keogh. Time series shapelets: a new primitive for data mining. In *Proceedings of the 15th ACM SIGKDD international conference on Knowledge discovery and data mining*, pages 947–956, 2009.
- [39] T. Zhang, H. Lu, and S. Z. Li. Learning semantic scene models by object classification and trajectory clustering. In *2009 IEEE conference on computer vision and pattern recognition*, pages 1940–1947. IEEE, 2009.
- [40] B. Zhao, H. Lu, S. Chen, J. Liu, and D. Wu. Convolutional neural networks for time series classification. *Journal of Systems Engineering and Electronics*, 28(1):162–169, 2017.

## 8 Appendix

### 8.1 Supplementary Material structure

The Supplementary Material is divided into two folders, one for the univariate experiments and one for the multivariate experiments. The results folder contains every result presented in the main paper and the Appendix, along with additional information for each set of experiments performed. Every model and window combination contains, for each dataset, the average accuracy over all runs of the same experiment, as well as the minimum/maximum accuracies and the standard deviation. These do not include the results from [16], which themselves are available on [14]. We do, however, include the script that was used to extract the results from the raw results posted on [14].

We include the processed data from the multivariate experiment, but due to size constraints, do not include any of the raw data nor any of the processed UCR data. The raw data can be obtained from [36] (<https://github.com/GlobalFishingWatch/training-data>) and [15] ([https://www.cs.ucr.edu/~eamonn/time\\_series\\_data\\_2018/](https://www.cs.ucr.edu/~eamonn/time_series_data_2018/)), and we include all extraction scripts (with listed in order) used in obtaining them. Those interested in doing so should only need to specify paths. However, it is important to note that both raw datasets (and the processed UCR dataset) are quite large. This may render personal verification infeasible without sufficient resources, though please note that none of the results were derived with GPUs.

### 8.2 Hyperparameters

The following hyperparameters were used for both univariate and multivariate tests. All variable names follow the same convention as in [33]

- KNN
  - n\_neighbors: 1, 2, 4, 6, 8, 10
  - weights: 'uniform', 'distance'
  - p: 1, 2
- SVM
  - C: 0.1, 1, 10
  - kernel: 'linear', 'rbf', 'poly'
  - degree: 2

### 8.3 Univariate comparison results

#### 8.3.1 Quantiles

We employ the following quantiles: 0.001, 0.01, 0.1, 0.2, 0.3, 0.4, 0.5, 0.6, 0.7, 0.8, 0.9, 0.99, 0.999.

We explicitly give the formatted average accuracy scores for the UCR 2018 archive, which includes the UCR/UEA datasets. All results are presented in Table 4. We omit the Crop dataset in our analysis due to memory constraints on available resources; this dataset is by far the largest dataset within the archive, with 7200 samples in the training set and 16800 in the test set, which resulted in out of memory issues when attempting to train the SVM models for multiple windows. These results are available for the 1-Window models in the Supplementary Material.

Note that the results in [16, 14] only run each experiment five times for each dataset used, hence accounting for any discrepancy with previous results. To ensure fair comparison, the results we list in Table 4 are also based on five iterations rather than the ten used for the UCR/UEA dataset in Section 4. This will inevitably create some discrepancy in numbers (more so for the deep learning methods based on comparing our results with those in [16, 14]); in terms of actual accuracy score, this is somewhat minor, though this may affect relative ranking results such as those in Table 2. We nevertheless chose in both the main paper (and the remainder of the Appendix) to focus on the UCR/UEA archive because of lower standard deviations.

Nevertheless, we see when recomputing relative rankings for the entire UCR 2018 archive (minus Crop) in Table 5 that the KNN and SVM models still do well. The major reason for the sharp increase in both high and low ranks is due to the additional datasets in the UCR 2018 archive, for which these

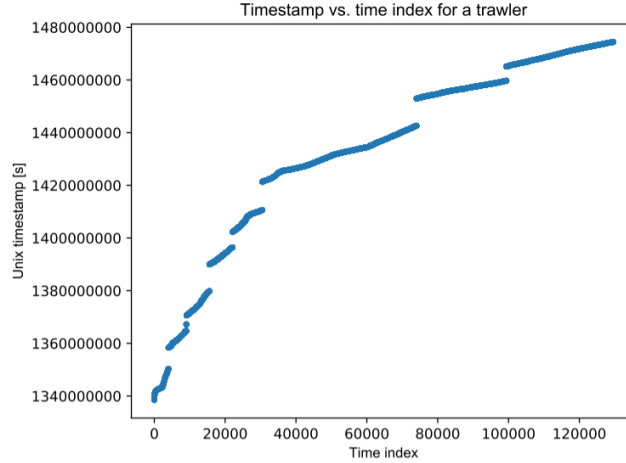
Table 4: Average accuracy of KNN and SVM with proposed features relative to the top 3 deep learning architectures from [16] every dataset (minus Crop) from the UCR 2018 archive.

Dataset	Top1	Top2	Top3	DIST_KNN	DIST_KNN_2	DIST_KNN_4	DIST_KNN_6	DIST_SVM	DIST_SVM_2	DIST_SVM_4	DIST_SVM_6
50Words	0.7402	0.7081	0.6585	0.4879	0.6888	0.7495	0.7473	0.5314	0.7380	0.7512	<b>0.7604</b>
ACSF1	0.9160	0.8980	0.5920	0.7180	0.6800	0.6700	0.9320	0.7220	0.6700	0.6600	<b>0.9920</b>
Adiac	<b>0.8414</b>	0.8332	0.6205	0.7366	0.7120	0.7059	0.0281	0.7601	0.7601	0.7739	0.0327
AllGestureWimoteX	<b>0.7406</b>	0.7134	0.5220	0.1000	0.1186	0.2897	0.1311	0.1000	0.1374	0.2900	0.1174
AllGestureWimoteY	<b>0.7937</b>	0.7832	0.6003	0.1000	0.1337	0.7209	0.0896	0.1000	0.1349	0.3231	0.0906
AllGestureWimoteZ	<b>0.7257</b>	0.6920	0.5163	0.1000	0.1254	0.2994	0.0666	0.1000	0.1286	0.3074	0.0449
ArrowHead	<b>0.8434</b>	0.8377	0.7840	0.7429	0.7657	0.8149	0.2137	0.7806	0.8343	0.7600	0.2491
Beef	0.7667	0.7533	0.7133	0.5667	0.5867	0.6067	<b>1.0000</b>	0.6333	0.7533	0.8000	<b>1.0000</b>
BeetleFly	0.9100	0.9000	0.8800	0.8500	0.8600	0.9000	<b>1.0000</b>	0.8900	0.7000	0.8200	<b>1.0000</b>
BirdChicken	0.9400	0.8800	0.7400	0.9000	0.9000	0.9000	<b>1.0000</b>	0.9000	0.9000	0.9000	<b>1.0000</b>
BME	0.9987	0.9467	0.9053	0.6667	0.9933	0.9600	0.2920	0.6867	<b>1.0000</b>	<b>1.0000</b>	0.4467
Car	<b>0.9167</b>	0.9133	0.7833	0.6900	0.8067	0.7333	0.1833	0.7167	0.8700	0.8467	0.1833
CBF	<b>0.9958</b>	0.9938	0.9773	0.8393	0.9627	0.9600	0.4936	0.9233	0.9811	0.9700	0.5009
Chinatown	<b>0.9796</b>	0.9784	0.9773	0.7411	0.9067	0.9534	0.5773	0.8338	0.8980	0.8980	0.6140
ChlorineConcentration	<b>0.8528</b>	0.8165	0.7999	0.5896	0.6627	0.6948	0.4685	0.6060	0.6591	0.7029	0.5326
CinCECGTorso	0.8378	0.8375	0.8288	0.6616	0.7819	0.8232	0.2887	0.7610	0.8891	<b>0.9268</b>	0.2210
Coffee	<b>1.0000</b>	<b>1.0000</b>	<b>1.0000</b>	0.9643	0.9286	0.9643	0.9571	0.9643	<b>1.0000</b>	<b>1.0000</b>	0.9643
Computers	0.8192	0.8056	0.6408	0.7184	0.6912	0.6328	<b>1.0000</b>	0.7480	0.6600	0.6080	0.9904
CricketX	<b>0.7990</b>	0.7944	0.6436	0.5605	0.5651	0.6308	0.0781	0.6513	0.6308	0.6718	0.0769
CricketY	<b>0.8103</b>	0.7928	0.6518	0.5179	0.6072	0.6436	0.0672	0.5918	0.6072	0.7385	0.0821
CricketZ	<b>0.8097</b>	0.8087	0.6508	0.5949	0.6041	0.6431	0.0903	0.6513	0.6821	0.6846	0.0615
DiatomSizeReduction	<b>0.9542</b>	0.9137	0.9092	0.8693	0.8922	0.9314	0.4170	0.8438	0.9150	0.9346	0.2719
DistalPhalanxOutlineAgeGroup	<b>0.7612</b>	0.7583	0.7295	0.6547	0.6863	0.6791	0.7022	0.7583	0.7482	0.7338	0.7338
DistalPhalanxOutlineCorrect	0.7725	0.7703	0.7601	0.7283	0.7310	0.7268	0.7014	0.7681	0.7522	0.7662	0.7464
DistalPhalanxTW	<b>0.6950</b>	0.6935	0.6849	0.6658	0.6187	0.6273	0.6402	0.6489	0.6489	0.6691	0.6532
DodgerLoopDay	<b>0.5925</b>	0.4875	0.3125	0.3475	0.4050	0.4025	0.4450	0.4575	0.4550	0.4750	0.5275
DodgerLoopGame	<b>0.8768</b>	0.8652	0.8159	0.6812	0.6986	0.6812	0.7333	0.6667	0.7319	0.7899	0.7899
DodgerLoopWeekend	<b>0.9826</b>	0.9783	0.9783	0.8913	0.9449	0.9522	0.9623	0.8333	0.9014	0.9159	0.9493
Earthquakes	0.7482	0.7482	0.7396	<b>0.7583</b>	0.7583	0.7583	0.7439	0.7496	0.7482	0.7482	0.7482
ECG200	<b>0.9140</b>	0.8880	0.8840	0.7700	0.8120	0.8300	0.8300	0.8020	0.8460	0.8140	0.8540
ECGS000	0.9415	0.9400	0.9351	0.9352	0.9408	0.9366	<b>0.9435</b>	0.9362	0.9376	0.9370	0.9355
ECGFiveDays	<b>0.9854</b>	0.9728	0.9663	0.8223	0.8420	0.8757	0.9117	0.8611	0.9106	0.9338	0.9466
ElectricDevices	<b>0.7279</b>	0.7065	0.7024	0.5382	0.5792	0.5840	0.6029	0.5055	0.6078	0.6043	0.6094
EOGHorizontalSignal	<b>0.5994</b>	0.5646	0.4320	0.4022	0.4138	0.4171	0.5169	0.4619	0.5166	0.5416	0.5416
EOGVerticalSignal	0.4464	0.4453	0.4177	0.3475	0.3420	0.3586	0.3575	0.4017	0.3862	<b>0.4646</b>	0.4530
EthanolLevel	0.7584	0.5584	0.5548	0.2556	0.2712	0.4256	0.4200	0.4356	0.4860	<b>0.7792</b>	0.7388
FaceAll	<b>0.9375</b>	0.8667	0.7943	0.5960	0.7343	0.7450	0.7497	0.7497	0.7751	0.8172	0.7595
FaceFour	<b>0.9545</b>	0.9295	0.9045	0.6591	0.5682	0.5795	0.7045	0.7159	0.5636	0.5682	0.7614
FacesUCR	<b>0.9542</b>	0.9434	0.8727	0.7010	0.7571	0.7571	0.8274	0.8569	0.8239	0.8566	0.8922
Fish	<b>0.9806</b>	0.9611	0.8777	0.7623	0.7920	0.8400	0.8720	0.8686	0.9086	0.8549	0.9246
FordA	<b>0.9370</b>	0.9283	0.9141	0.7595	0.7617	0.7652	0.7602	0.8265	0.8188	0.8318	0.8402
FordB	<b>0.8131</b>	0.7770	0.7723	0.5765	0.5943	0.6220	0.6017	0.6444	0.6069	0.6410	0.6654
FreezerRegularTrain	<b>0.9985</b>	0.9968	0.9867	0.9596	0.9575	0.9714	0.9578	0.9865	0.9937	0.9947	0.9933
FreezerSmallTrain	0.9171	0.8322	0.7387	0.9144	0.9140	0.9140	0.9140	0.8596	0.9202	<b>0.9719</b>	0.9719
Fungi	0.9613	0.9344	0.8634	0.6935	0.8280	0.9462	<b>0.9677</b>	0.6667	0.7581	0.8602	0.9194
GestureMidAirD1	<b>0.6985</b>	0.6954	0.5754	0.0385	0.1631	0.4923	0.4908	0.0385	0.2000	0.5231	0.5800
GestureMidAirD2	<b>0.6677</b>	0.6308	0.5754	0.0385	0.1554	0.3338	0.4092	0.0385	0.1769	0.4308	0.4015
GestureMidAirD3	<b>0.3815</b>	0.3677	0.3400	0.0385	0.0892	0.2646	0.2692	0.0385	0.1077	0.2846	0.2892
GesturePebbleZ1	<b>0.9012</b>	0.8802	0.8442	0.1570	0.3105	0.5000	0.5000	0.5000	0.5000	0.5000	0.5000
GesturePebbleZ2	<b>0.8430</b>	0.7962	0.7810	0.1557	0.3418	0.3481	0.3797	0.1582	0.4051	0.4000	0.4494
GunPoint	<b>1.0000</b>	0.9907	0.9893	0.9573	0.9800	0.9800	0.9627	0.9813	0.9747	0.9933	0.9733
GunPointAgeSpan	<b>0.9968</b>	0.9956	0.9646	0.9747	0.9842	0.9918	0.9848	0.9715	0.9842	0.9778	0.9380
GunPointMaleVersusFemale	0.9968	0.9924	0.9880	0.9873	0.9842	<b>0.9968</b>	0.9873	0.9905	0.9867	0.9899	0.9892
GunPointOldVersusYoung	0.9992	0.9986	0.9752	0.9968	0.9968	<b>1.0000</b>	<b>1.0000</b>	<b>1.0000</b>	<b>1.0000</b>	<b>1.0000</b>	<b>1.0000</b>
Ham	<b>0.7676</b>	0.7581	0.7200	0.4457	0.5962	0.5600	0.5543	0.5562	0.6990	0.6476	0.6914
HandOutlines	<b>0.9141</b>	0.9135	0.9043	0.6865	0.7476	0.8292	0.7724	0.7892	0.8405	0.8459	0.8378
Haptics	0.5097	0.4896	0.4253	0.4169	0.4455	0.4558	0.4344	0.4526	0.5227	0.5045	<b>0.5357</b>
Herring	0.6438	0.6250	0.6000	0.5000	0.4906	<b>0.6488</b>	0.6488	0.6438	0.6438	0.6438	0.6188
HouseTwenty	0.9832	0.9815	0.9908	0.8992	0.9412	0.9412	0.9092	0.9496	0.9748	<b>0.9832</b>	0.9748
InlineSkate	0.3771	0.3345	0.3316	<b>0.5291</b>	0.5145	0.4858	0.4582	0.4818	0.5127	0.4284	0.4287
InsectEPGRegularTrain	0.9992	0.9976	0.8811	<b>1.0000</b>	0.9880	0.9960	0.9880	<b>1.0000</b>	0.9960	0.9960	0.9880
InsectEPGSmallTrain	0.6819	0.6811	0.6273	<b>1.0000</b>	0.9936	0.9880	0.9920	0.9960	0.9960	0.9880	0.9759
InsectWingbeatSound	<b>0.6298</b>	0.6042	0.5868	0.2618	0.4386	0.4879	0.5112	0.4888	0.5328	0.5905	0.5905
ItalyPowerDemand	<b>0.9664</b>	0.9638	0.9629	0.7351	0.8439	0.9320	0.9415	0.7874	0.8967	0.9549	0.9549
LargeKitchenAppliances	<b>0.9029</b>	0.9013	0.7840	0.7792	0.7253	0.6635	0.6629	0.8240	0.7627	0.6853	0.6880
Lightning2	0.7803	0.7344	0.7148	0.7705	0.7574	0.7967	0.8033	<b>0.8197</b>	0.7508	0.7541	0.7148
Lightning7	<b>0.8274</b>	0.8247	0.6959	0.5890	0.6932	0.7397	0.7507	0.7205	0.7397	0.7671	0.7370
Mailat	<b>0.9736</b>	0.9671	0.9231	0.9202	0.9322	0.9522	0.9531	0.9705	0.9480	0.9505	0.9505
Meat	<b>0.9900</b>	0.9700	0.9133	0.8867	0.9333	0.9567	0.9200	0.9667	0.9500	0.9833	0.9500
MedicalImages	<b>0.7784</b>	0.7697	0.7187	0.7421	0.6966	0.6939	0.6534	0.7658	0.7513	0.7200	0.7145
MelbournePedestrian	<b>0.9123</b>	0.9092	0.8840	0.8207	0.8893	0.9029	0.9080	0.8369	0.8801	0.9016	0.8967
MiddlePhalanxOutlineAgeGroup	<b>0.5779</b>	0.5766	0.5584	0.4325	0.4325	0.4468	0.4338	0.3805	0.4545	0.5000	0.4675
MiddlePhalanxOutlineCorrect	<b>0.8614</b>	0.7950	0.7945	0.5361	0.5457	0.5407	0.6017	0.6398	0.6437	0.6818	0.5614
MiddlePhalanxTW	0.5974	0.5688	0.5623	0.5234	0.5403	0.5351	0.5558	0.5714	0.5649	0.5909	<b>0.6169</b>
MixedShapesRegularTrain	0.9729	0.9549	0.9067	0.9236	0.9559	0.9733	0.9476	0.9654	0.9600	<b>0.9748</b>	0.9748
MixedShapesSmallTrain	0.9165	0.9344	0.8411	0.8701	0.9066	0.9295	0.9339	0.8987	0.9316	0.9302	<b>0.9460</b>
MoteStrain	<b>0.9358</b>	0.9240	0.8853	0.8069	0.8641	0.8722	0.8874	0.8858	0.8922	0.8658	0.8986
NonInvasiveFetalECGThorax1	<b>0.9863</b>	0.9414	0.9148	0.8184	0.8397	0.8480	0.8865	0.9069	0.9219	0.9105	0.9105
NonInvasiveFetalECGThorax2	<b>0.9531</b>	0.9436	0.9184	0.8286	0.8414	0.8521	0.8416	0.8826	0.8941	0.8961	0.8901
OliveOil	0.8467	0.8400	0.7200	0.8333	0.8200	0.8867	0.8533	0.8667	0.8333	<b>0.9000</b>	<b>0.9000</b>
OSULeaf	<b>0.9802</b>	0.9785	0.6281	0.8273	0.7719	0.7752	0.8033	0.9008	0.8488	0.8058	0.8595
PhalangesOutlinesCorrect	<b>0.8452</b>	0.8177	0.7991	0.7089	0.7196	0.7168	0.7291	0.7576	0.7494	0.7669	0.7739
Phoneme	<b>0.3334</b>	0.3280	0.1743	0.1943	0.2326	0.2680	0.2680	0.2398	0.2483	0.2848	0.2832
PickupGestureWimoteZ	<b>0.7440</b>	0.7040	0.6160	0.1000	0.1840	0.3760	0.5000	0.1000	0.2200	0.4840	0.6080
PigAirwayPressure	0.4058	0.1721	0.1625	<b>0.4760</b>	0.3606	0.1635	0.1538	0.4231	0.3269	0.1538	0.1635
PigArtPressure	<b>0.9913</b>	0.9865	0.6692	0.9519	0.9279	0.8750	0.8510	0.9231	0.9135	0.8365	0.8365
PigCVP	<b>0.9183</b>	0.8308	0.5192	0.6731	0.6442	0.3048	0.3029	0.5817	0.5769	0.3798	0.3365
PLAID	<b>0.9404</b>	0.9039</									

Table 5: Number of times a given model and feature combination achieves a given rank relative to seven deep learning models in [16] that we compare to for the UCR 2018 dataset (minus Crop).

Model	1st	2nd	3rd	4th	5th	6th	7th	8th
1-Window KNN	26	6	8	11	6	10	16	45
2-Window KNN	25	6	18	16	5	15	8	35
4-Window KNN	32	7	16	15	8	9	10	31
6-Window KNN	36	3	13	10	7	6	12	41
1-Window SVM	30	6	20	7	16	8	16	35
2-Window SVM	35	6	25	9	9	5	6	33
4-Window SVM	39	6	22	13	11	3	7	39
6-Window SVM	41	5	17	8	8	4	4	41
Best KNN	39	8	14	17	7	5	12	26
Best SVM	47	6	23	10	6	4	8	24

Figure 2: The time values (in Unix time) of the first timestamps for a trawler. Each unit is one second.



models seem to either perform very well or very poorly. The best SVM, as well as SVMs with two and four windows are within the top three for over half of the datasets in the collection.

## 8.4 Vessel classification details

### 8.4.1 Incorporating sampling rate

Each vessel trajectory in [36] is sampled nonuniformly and asynchronously of one another. The sampling rate for a given vessel is correlated with ocean traffic: if a vessel is around a large number of other vessels, then its sampling rate is more likely to decrease [21]. The number of neighbors of a given vessel (in some radius) was incorporated as a feature used in [21]. Given the lack of data that we have access to compared to [21], it is not reasonable to expect that such a feature will contain as much information in our case. Nevertheless, the sampling rate may act as a proxy that allows us to incorporate neighbor information. Thus, in addition for the geometric features considered, we also consider distributions based on the sampling rate. More specifically, we consider distributions of lengths of times in which each vessel falls into one of three classifications determined by its speed and sampling rate: active, inactive, and unknown.

Active time periods are those in which the vessel is moving at a speed greater than or equal to a predefined threshold, whereas inactive time periods are those where the vessel is moving at a speed less than said threshold. Note that it is natural for a vessel to be periodically inactive (e.g. not in use). We specifically chose 0.4 knots as the threshold. For active time periods, all previously mentioned geometric quantities are relevant. For inactive times, the only relevant quantity is the length of period of inactivity; vessels are otherwise almost stationary.

We define an unknown time period to be one in which the amount of time between consecutive samples of a trajectory is at least a minimum threshold; we chose 90 minutes. The length of time between any two samples of a vessel can be quite high; Figure 2 shows the potential length of gaps for one vessel. Distribution-wise, we consider the distribution of the lengths of time between samples provided that the time between samples is at least 90 minutes. This will act as a proxy for the amount of neighbors a vessel has at any point of time.

#### 8.4.2 Other geometric features

In addition to the geometric features listed in Section 3, we include a number of other relevant features within our analysis. Two features of interest in this vessel classification problem, distance to shore and distance to port, are given for each trajectory at each time. We also use two variants of the curvature feature proposed in Section 3: the one proposed, and one obtained without any Laplacian smoothing after differentiating. Using both in tandem gives a multiscale notion of curvature, which initial experiments found important for establishing optimal performance.

#### 8.4.3 Quantiles

We employ the following quantiles: 0.001, 0.01, 0.05, 0.1, 0.25, 0.5, 0.75, 0.9, 0.95, 0.99, 0.999.

#### 8.4.4 Preprocessing

Not all of the 1258 trajectories available in [36] are immediately usable. A number of these trajectories, for example, do not have a well defined vessel label. Per the supplementary information in [21], this would suggest a classification of "other fishing" or "gear/buoy" for each such vessel. Given that the former represents a catch-all category for fishing vessels (for which motion pattern is decidedly unclear) and those in the latter category are not actually vessels, we chose to ignore these in subsequent algorithm development. Note that the performance analysis in [21] did not explicitly consider the gear/buoy class, and achieved approximately 50% classification accuracy in test, so our decision is not without practical merit. We also chose to remove vessels that did not exhibit any periods of inactivity or any long sampling times; only seven vessels satisfied this property, creating minimal effect. This leaves 1107 trajectories remaining.

Given the length of time that the trajectories span, it is natural that the vessels are motionless for some amount of time. Though the length of such time is of interest, other aspects of the behavior of the vessel are clearly not meaningful. Thus, for each of the 1107 vessels, we first determine if the vessel's speed is fast enough to indicate movement (we chose 0.4 knots as the threshold).

As previously mentioned, the average such length is itself time dependent. Furthermore, as Figure 2 showed, the gaps can be quite large. It is not reasonable to assume the behavior before such a gap is similar to that after such a gap. We thus segment the trajectory as follows. We divide each section of the trajectory where the timestamps are consecutively moving or otherwise into subintervals, where two consecutive timestamps are within the same interval if there is at most a 90 minute (5400 second) difference between them. As we are expressly interested in the length between such large time gaps, we record them as they are observed. We keep the intervals (and corresponding portion of the trajectories) if they contain at least four timestamps, and ignore those that have three or fewer timestamps. These segments are ignored because of their tendency to exhibit anomalous behavior.

Features are derived in two different ways depending on whether the vessel was determined to be actively moving. For the subtrajectories where the vessel was not moving, the only feature of interest is the length of time of such an event. We record this by looking at the difference between the first and last timestamp, and then ignore the segment for the remainder of our analysis.

For the subtrajectories where the vessel is in motion, we first perform piecewise linear interpolation along the time interval in which the subtrajectory is defined. Unlike for the univariate setting, we employ ten iterations of Laplacian smoothing to smoothen our data; this was chosen empirically to remove all possible noise that might have had negative effects in subsequent analysis.

We then constructed samples for each distribution of geometric features by extracting the average value of the interpolated quantities over a ten minute window. We also included the average values for portions of subtrajectories less than ten minutes (which only occurs towards the end values)

Figure 3: Confusion matrices for one 10-fold nested cross validation experiment on the vessel classification dataset. Left: KNN, Right: SVM

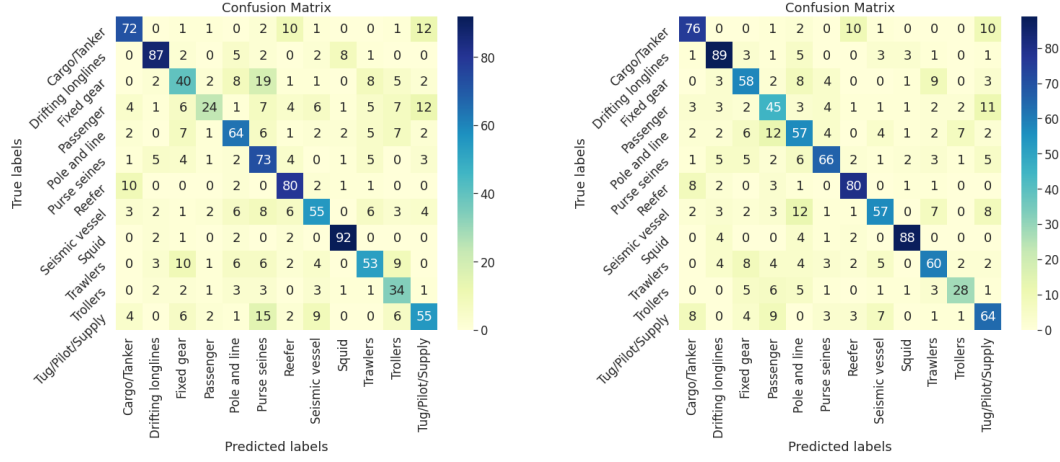
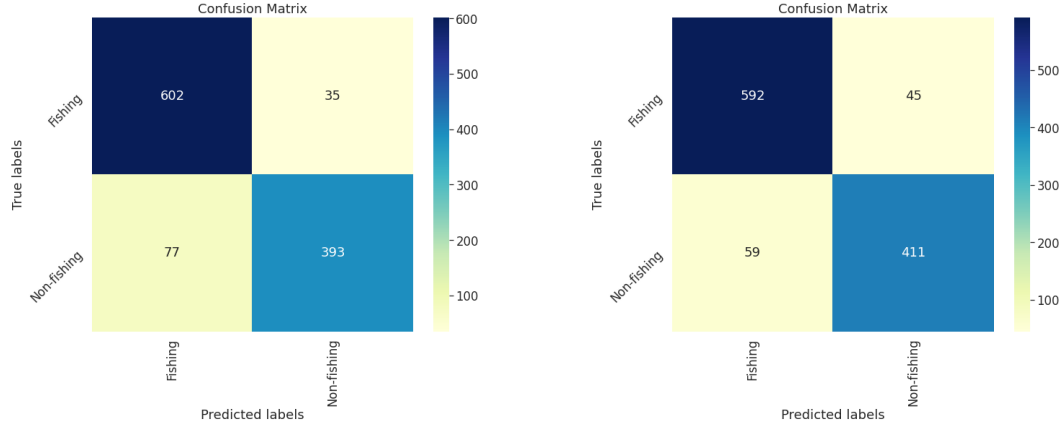


Figure 4: Confusion matrices for one 10-fold nested cross validation experiment on the vessel classification dataset for the binary problem of whether a vessel is involved in fishing. Left: KNN, Right: SVM



as samples for our distributions. Samples for values of distributions related to sampling rate are computed in the obvious way: measure the relevant lengths of time.

All features are Z-normalized.

#### 8.4.5 Confusion matrices

In Figure 3, we show the confusion matrices for both KNN and SVM for a fixed, illustrative run of 10-fold nested cross validation. We have already established in Section 4 that both KNN and SVM yield somewhat surprising accuracy despite the lack of data. Looking at the confusion matrices, we see that perhaps some mislabeling is warranted. In particular, we note three main types of mislabeling: fishing vessels getting labeled as other types of fishing vessels, reefers (refrigerated cargo) and cargo vessels getting confused, and tugboats getting confused with various classes. It is reasonable to expect that different types of fishing vessels may exhibit similar movement patterns; the same is true for reefers and cargo vessels. High confusion with tug/pilot/supply is also interesting but not surprising; a ship broken down at sea that requires a tugboat is likely to exhibit similar movement patterns to a tugboat.



To give some credence to our claim that mislabeling of one fishing vessel with another is reasonable, we also show in Figure 4 the confusion matrices for the binary classification problem of whether a vessel is involved in fishing. Here, the KNN model achieves an accuracy of 89.88% while the SVM model achieves an accuracy of 90.61%. Again, note that this is with a nested cross validation procedure on approximately two percent of the data available in [21], the model in which achieves a near-perfect accuracy score. This further supports that our features are accurately capturing quantities of interest.

## 8.5 Details of empirical studies

### 8.5.1 Amount of smoothing

Table 6 displays the average results after ten training-validation-test experiments (with 10-fold cross validation) for both KNN and SVM models with one window. The number in each column refers to the number of iterations of Laplacian smoothing used in the feature extraction procedure. As mentioned in the text, there does not seem to be a consistent rule in terms of how much smoothing matters. We thus reason that any such choice should ultimately be dataset-dependent.

### 8.5.2 Parameter ablation

Table 7 shows the average effect of the removal of different sets of parameters on the accuracy of both KNN and SVM classifiers for the features given in the GFW dataset. The average is taken over thirty iterations of the 10-fold nested cross-validation procedure. By low, high, and mid quantiles, we mean the lowest four, highest four, and middle three considered of those previously mentioned. The removal of both location (position), speed, and the middle quantiles negatively effect both classifiers. This is unsurprising as the information contained within these (the value of the time series, the rate of change of the time series, and the typical behavior of all quantities) is important basic information.

What is interesting is the effect of the different parameters on the two classifiers. KNN seems to improve by removing most other information. Though this may seem surprising at first glance, we note that the coordinates of the individual features we use can be highly correlated with one another. Given this and general high dimensionality concerns, it is possible that 1-norm and 2-norm distances are not appropriate without additional dimensionality reduction, so that any feature removal may improve performance. We did not test this in detail. SVM, on the other hand, seems to negatively perform without most of the geometric features listed. The initial hypothesis of improvement with multiscale curvature information is not verified given negligible improvement with either rough or smoothed curvature (but not both) removed. Inactivity was also surprisingly not helpful in improving accuracy, contradicting some of the information in [21]. For statistics employed, only removing low and mid quantiles had a notable negative effect on performance, with every other feature having negligible impact.

### 8.5.3 Specific window effect

Table 8 and Table 9 show the performance most of the UCR/UEA dataset when training on one of six continuous disjoint windows of data. Due to SVM convergence issues, we did not display the results for ElectricDevices and the Proximal datasets. These datasets feature large segments for which many of the time series in these datasets are constants. Given that many of the quantities of interest we investigate involve derivatives, this creates a large amount of redundant information, rendering searches on a number of these windows useless.

As mentioned in Section 4, restricting to particular windows does not seem to improve classifier performance. However, it is extremely interesting to note the high amount of classification accuracy obtainable by restricting to these individual windows. In particular, a number of datasets achieve perfect accuracy when restricting to these windows, giving credence to the idea of local information playing an important role in some cases. Nevertheless, in other datasets, it's quite clear that local information is not remotely sufficient to train an accurate classifier.

Table 6: The effect of different amounts of Laplacian smoothing on classification accuracy

	KNN_0_Smooth	KNN_1_Smooth	KNN_2_Smooth	SVM_0_Smooth	SVM_1_Smooth	SVM_2_Smooth
50Words	0.4716	0.4879	0.4793	0.5292	0.5310	0.5356
Adiac	0.6793	0.7289	0.7335	0.7565	0.7593	0.7517
ArrowHead	0.6766	0.7429	0.7417	0.6914	0.7703	0.7920
Beef	0.5667	0.5667	0.6300	0.7000	0.6267	0.6067
BeetleFly	0.8500	0.8500	0.7500	0.8600	0.8900	0.9500
BirdChicken	1.0000	0.9000	0.9000	0.9000	0.9000	0.9000
Car	0.7750	0.6900	0.7267	0.8367	0.7167	0.7333
CBF	0.7599	0.8411	0.8771	0.8389	0.9233	0.9140
ChlorineConcentration	0.6542	0.5982	0.5732	0.6273	0.6060	0.5790
CinCECGTorso	0.7014	0.6616	0.6380	0.7446	0.7490	0.7114
Coffee	0.9321	0.9643	0.9357	0.9643	0.9643	1.0000
Computers	0.7648	0.7084	0.6960	0.7300	0.7480	0.7020
CricketX	0.5805	0.5605	0.5510	0.6367	0.6538	0.6238
CricketY	0.5362	0.5179	0.5744	0.6308	0.5946	0.5823
CricketZ	0.6044	0.5974	0.5538	0.6385	0.6513	0.6162
DiatomSizeReduction	0.9346	0.8693	0.9281	0.9216	0.8438	0.9248
DistalPhalanxOutlineAgeGroup	0.6842	0.6583	0.6986	0.7388	0.7568	0.7633
DistalPhalanxOutlineCorrect	0.7417	0.7261	0.7297	0.7522	0.7681	0.7587
DistalPhalanxTW	0.6237	0.6065	0.6194	0.6640	0.6791	0.6432
Earthquakes	0.7460	0.7554	0.7468	0.7367	0.7496	0.7403
ECG200	0.7780	0.7730	0.7780	0.7350	0.7800	0.7390
ECG5000	0.9328	0.9348	0.9315	0.9321	0.9362	0.9331
ECGFiveDays	0.8153	0.8223	0.8188	0.7621	0.8697	0.8955
ElectricDevices	0.5547	0.5384	0.5377	0.5850	0.5055	0.5910
FaceAll	0.6187	0.5985	0.5962	0.7302	0.7497	0.7426
FaceFour	0.5909	0.6591	0.7045	0.5966	0.7159	0.7273
FacesUCR	0.6794	0.7019	0.7083	0.7259	0.7395	0.7679
Fish	0.7309	0.7417	0.8080	0.8480	0.8686	0.8766
FordA	0.7714	0.7592	0.7433	0.8303	0.8265	0.8690
FordB	0.5483	0.5759	0.5885	0.5965	0.6444	0.6914
GunPoint	0.9100	0.9527	0.9820	0.9387	0.9813	0.9867
Ham	0.5295	0.4457	0.4952	0.6038	0.5724	0.5962
HandOutlines	0.7054	0.6862	0.7203	0.7892	0.7914	0.7832
Haptics	0.3659	0.4188	0.4146	0.3987	0.4532	0.4620
Herring	0.4906	0.5031	0.5844	0.5938	0.6594	0.5781
InlineSkate	0.5455	0.5291	0.5655	0.5555	0.4818	0.5636
InsectWingbeatSound	0.2649	0.2622	0.2606	0.3539	0.3511	0.3760
ItalyPowerDemand	0.7921	0.7407	0.7308	0.8113	0.7842	0.7990
LargeKitchenAppliances	0.7547	0.7803	0.7963	0.8123	0.8240	0.7427
Lightning2	0.6820	0.7689	0.7869	0.7738	0.8115	0.7311
Lightning7	0.5589	0.6055	0.6096	0.6027	0.7151	0.7014
Mallat	0.9458	0.9159	0.9070	0.9467	0.9305	0.9363
Meat	0.7717	0.8833	0.9133	0.9167	0.9667	0.9167
MedicalImages	0.6970	0.7400	0.7121	0.7645	0.7658	0.7632
MiddlePhalanxOutlineAgeGroup	0.4325	0.4390	0.4188	0.4779	0.4117	0.4909
MiddlePhalanxOutlineCorrect	0.5746	0.5361	0.5498	0.6900	0.6110	0.6323
MiddlePhalanxTW	0.5162	0.5292	0.5390	0.6039	0.5714	0.5377
MoteStrain	0.8067	0.8039	0.8215	0.8395	0.8858	0.8994
NonInvasiveFetalECGThorax1	0.7902	0.8195	0.8349	0.8778	0.8960	0.9009
NonInvasiveFetalECGThorax2	0.8281	0.8276	0.8342	0.8902	0.8826	0.8876
OliveOil	0.7767	0.8333	0.8133	0.8133	0.8667	0.8633
OSULeaf	0.8649	0.8306	0.8140	0.9120	0.9008	0.8537
PhalangesOutlinesCorrect	0.7348	0.7107	0.6946	0.7506	0.7576	0.7517
Phoneme	0.2225	0.1985	0.2062	0.2333	0.2367	0.2333
Plane	0.9905	1.0000	1.0000	0.9905	1.0000	1.0000
ProximalPhalanxOutlineAgeGroup	0.8112	0.8459	0.8371	0.8463	0.8439	0.8351
ProximalPhalanxOutlineCorrect	0.8045	0.7814	0.8000	0.8007	0.8110	0.8144
ProximalPhalanxTW	0.7620	0.7522	0.7629	0.7663	0.7615	0.7288
RefrigerationDevices	0.5037	0.4747	0.5013	0.4933	0.5125	0.4827
ScreenType	0.4587	0.3995	0.3656	0.5227	0.4853	0.4027
ShapeletSim	0.9367	0.9172	0.8256	0.9494	0.9694	0.9222
ShapesAll	0.7817	0.8155	0.8123	0.8013	0.8433	0.8535
SmallKitchenAppliances	0.7173	0.7307	0.7227	0.7403	0.7744	0.7787
SonyAIBORobotSurface1	0.7413	0.7770	0.7920	0.7829	0.7953	0.7987
SonyAIBORobotSurface2	0.9140	0.9064	0.9213	0.9308	0.9224	0.9444
StarLightCurves	0.9760	0.9760	0.9765	0.9774	0.9779	0.9778
Strawberry	0.9081	0.9151	0.9216	0.9514	0.9541	0.9470
SwedishLeaf	0.8658	0.9064	0.9126	0.9141	0.9293	0.9310
Symbols	0.9099	0.8750	0.8481	0.9085	0.9116	0.9045
SyntheticControl	0.8357	0.8157	0.8477	0.9027	0.9080	0.9130
ToeSegmentation1	0.7395	0.7118	0.7408	0.8228	0.7982	0.8711
ToeSegmentation2	0.7023	0.7100	0.6938	0.5923	0.6231	0.6077
Trace	0.8680	0.9180	0.9520	0.9900	0.9800	1.0000
TwoLeadECG	0.9404	0.9363	0.9603	0.9911	0.9877	0.9895
TwoPatterns	0.7123	0.7083	0.7096	0.7636	0.7680	0.7762
UWaveGestureLibraryAll	0.6516	0.6573	0.6474	0.7527	0.7357	0.7447
UWaveGestureLibraryX	0.7021	0.6900	0.6890	0.7279	0.7321	0.7166
UWaveGestureLibraryY	0.6269	0.6165	0.6066	0.6619	0.6415	0.6399
UWaveGestureLibraryZ	0.6365	0.6222	0.6150	0.6815	0.6803	0.6770
Wafer	0.9953	0.9942	0.9868	0.9990	0.9961	0.9936
Wine	0.6296	0.5778	0.5648	0.6333	0.5556	0.5185
WordSynonyms	0.4879	0.4911	0.4793	0.4687	0.4655	0.4734
Worms	0.6247	0.6558	0.6701	0.7221	0.7091	0.7364
WormsTwoClass	0.7662	0.7688	0.7597	0.7818	0.7792	0.7403
Yoga	0.7807	0.7864	0.7803	0.8003	0.8093	0.7910

Table 7: Ablation results for a fixed random seed on the GFW vessel dataset

Removed Features	KNN	Percent Change	Removed Features	SVM	Percent Change
None	0.6622	0.0000	All	0.6956	0.0000
Active Times	0.6793	2.5825	Active Times	0.6830	-1.8202
Inactive Times	0.6685	0.9511	Inactive Times	0.7028	1.0349
Unknown Times	0.6820	2.9956	Unknown Times	0.6865	-1.3057
Location	0.6504	-1.7785	Location	0.6532	-6.1011
Speed	0.6278	-5.1897	Speed	0.6486	-6.7545
Acceleration	0.6586	-0.5491	Acceleration	0.6883	-1.0478
Smoothed Curvature	0.6892	4.0840	Smoothed Curvature	0.6983	0.3826
Rough Curvature	0.6847	3.4000	Rough Curvature	0.7001	0.6440
All Curvatures	0.6847	3.4062	All Curvatures	0.6757	-2.8622
All Second Derivatives	0.6811	2.8521	All Second Derivatives	0.6766	-2.7374
Distance to Port	0.6703	1.2232	Distance to Port	0.6848	-1.5588
Distance to Shore	0.6739	1.7649	Distance to Shore	0.6848	-1.5588
Range	0.6793	2.5899	Range	0.7010	0.7782
Mean	0.6676	0.8101	Mean	0.6956	-0.0059
Std	0.6784	2.4439	Std	0.6974	0.2578
Skew	0.6775	2.3104	Skew	0.6983	0.3874
Kurtosis	0.6793	2.5862	Kurtosis	0.6992	0.5145
Low Quantiles	0.6567	-0.8324	Low Quantiles	0.6739	-3.1235
Mid Quantiles	0.6450	-2.6023	Mid Quantiles	0.6549	-5.8550
High Quantiles	0.6929	4.6356	High Quantiles	0.6974	0.02567

Table 8: The accuracy of KNN when training on individual windows

Model	KNN_Window_1	KNN_Window_2	KNN_Window_3	KNN_Window_4	KNN_Window_5	KNN_Window_6
50Words	0.4708	0.4738	0.4277	0.4152	0.4587	0.4648
Adiac	0.0348	0.0414	0.0348	0.0345	0.0332	0.0322
ArrowHead	0.2817	0.3640	0.2497	0.2760	0.1989	0.2577
Beef	1.0000	1.0000	0.9333	1.0000	1.0000	0.6333
BeetleFly	0.9900	1.0000	0.9700	0.9700	1.0000	1.0000
BirdChicken	0.8800	1.0000	1.0000	1.0000	0.9550	1.0000
Car	0.2033	0.1767	0.1733	0.1867	0.1850	0.1850
CBF	0.3546	0.4883	0.4962	0.2404	0.4952	0.4012
ChlorineConcentration	0.4767	0.4734	0.4597	0.4685	0.4643	0.4640
CinCECGTorso	0.2598	0.3001	0.2034	0.2770	0.2486	0.2495
Coffee	0.9000	0.7893	0.9393	0.9393	0.9643	0.7964
Computers	1.0000	1.0000	0.8172	0.8832	0.9320	1.0000
CricketX	0.0810	0.0556	0.0782	0.0646	0.0772	0.0838
CricketY	0.0810	0.0818	0.0703	0.0890	0.0800	0.0764
CricketZ	0.0841	0.0769	0.0918	0.0841	0.0813	0.0723
DiatomSizeReduction	0.3729	0.3647	0.3124	0.2533	0.3039	0.3366
DistalPhalanxOutlineAgeGroup	0.5719	0.5698	0.5957	0.7014	0.5381	0.5957
DistalPhalanxOutlineCorrect	0.6399	0.6047	0.6652	0.6971	0.5482	0.5913
DistalPhalanxTW	0.4820	0.5719	0.5065	0.6360	0.6043	0.6007
Earthquakes	0.7424	0.7410	0.7439	0.7453	0.7403	0.7388
ECG200	0.8190	0.8540	0.8150	0.7790	0.7200	0.7400
ECG5000	0.9286	0.9033	0.8040	0.8235	0.9249	0.9320
ECGFiveDays	0.6632	0.6619	0.8676	0.7672	0.7050	0.9034
FaceAll	0.6304	0.5746	0.5769	0.4570	0.4442	0.4002
FaceFour	0.4750	0.5682	0.6830	0.6886	0.4114	0.3182
FacesUCR	0.4201	0.5170	0.5141	0.6624	0.5407	0.5437
Fish	0.5720	0.7966	0.7423	0.7394	0.5886	0.3549
FordA	0.7004	0.6873	0.7365	0.6984	0.7024	0.6982
FordB	0.5763	0.5642	0.5737	0.5995	0.5727	0.5838
GunPoint	0.7160	0.9600	0.7273	0.8040	0.8347	0.8733
Ham	0.6352	0.5190	0.5619	0.5362	0.5981	0.4571
HandOutlines	0.7184	0.8232	0.7478	0.7146	0.7386	0.6335
Haptics	0.3429	0.4010	0.3828	0.3458	0.3873	0.3766
Herring	0.6016	0.5781	0.5609	0.5578	0.5719	0.5547
InlineSkate	0.3953	0.2533	0.2638	0.2836	0.2827	0.3978
InsectWingbeatSound	0.4399	0.4021	0.4052	0.3266	0.3095	0.2644
ItalyPowerDemand	0.6279	0.7944	0.8029	0.8047	0.9376	0.9322
LargeKitchenAppliances	0.5189	0.5021	0.6264	0.5640	0.5563	0.6120
Lightning2	0.6033	0.6213	0.7246	0.6393	0.6902	0.6377
Lightning7	0.3918	0.4027	0.4411	0.4671	0.6712	0.4740
Mallat	0.4956	0.6206	0.4333	0.5373	0.6944	0.6216
Meat	0.8750	0.8933	0.9983	0.8433	0.8783	0.8333
MedicalImages	0.6789	0.5276	0.5536	0.5172	0.5338	0.5639
MiddlePhalanxOutlineAgeGroup	0.3987	0.3669	0.3669	0.5318	0.4545	0.4032
MiddlePhalanxOutlineCorrect	0.4918	0.4708	0.5227	0.6168	0.4948	0.5320
MiddlePhalanxTW	0.4864	0.4760	0.5565	0.5597	0.5162	0.5292
MoteStrain	0.7738	0.8213	0.7577	0.7827	0.8147	0.6998
NonInvasiveFetalECGThorax1	0.7812	0.4126	0.4687	0.3384	0.4824	0.6038
NonInvasiveFetalECGThorax2	0.8419	0.4096	0.5115	0.3733	0.5253	0.7317
OliveOil	0.7067	0.8733	0.6733	0.9000	0.8967	0.7667
OSULeaf	0.6281	0.5657	0.5723	0.5463	0.5802	0.6570
PhalangesOutlinesCorrect	0.6414	0.6076	0.6824	0.7174	0.5988	0.5851
Phoneme	0.1439	0.1598	0.1626	0.1777	0.1543	0.1362
RefrigerationDevices	0.5032	0.5333	0.4237	0.4595	0.4403	0.4619
ScreenType	0.3395	0.3920	0.3299	0.3947	0.4765	0.4373
ShakeGestureWiimoteZ	0.5600	0.3280	0.3440	0.1840	0.1000	0.1000
ShapeletSim	0.5372	0.6106	0.5139	0.4806	0.5722	0.5150
ShapesAll	0.6367	0.6467	0.5817	0.6157	0.6533	0.6633
SmallKitchenAppliances	0.7429	0.6853	0.6787	0.6653	0.6909	0.6483
SonyAIBORobotSurface1	0.7255	0.7233	0.4735	0.6805	0.6556	0.6338
SonyAIBORobotSurface2	0.7487	0.8612	0.7470	0.7031	0.8135	0.7933
StarLightCurves	0.9492	0.9500	0.9170	0.9381	0.9240	0.9345
Strawberry	0.8568	0.9459	0.9119	0.9459	0.8192	0.8595
SwedishLeaf	0.7931	0.6930	0.7552	0.7664	0.7320	0.7645
Symbols	0.6030	0.8141	0.6990	0.8030	0.7397	0.7071
SyntheticControl	0.7920	0.7253	0.7407	0.7803	0.7183	0.7207
ToeSegmentation1	0.5737	0.6548	0.6180	0.6711	0.6039	0.6009
ToeSegmentation2	0.7677	0.5823	0.6923	0.7115	0.6531	0.6385
Trace	0.5350	0.6760	0.5700	0.6890	0.7170	0.3930
TwoLeadECG	0.6672	0.8306	0.9374	0.7199	0.6536	0.5890
TwoPatterns	0.3331	0.3712	0.3844	0.4045	0.5071	0.4035
UWaveGestureLibraryAll	0.7211	0.7467	0.6552	0.6774	0.6879	0.5911
UWaveGestureLibraryX	0.5088	0.6390	0.5861	0.5690	0.6056	0.5796
UWaveGestureLibraryY	0.4736	0.5628	0.5281	0.5251	0.5088	0.5257
UWaveGestureLibraryZ	0.5017	0.5948	0.5486	0.5204	0.5161	0.4902
Wafer	0.9933	0.9901	0.9640	0.9661	0.9852	0.9916
Wine	0.6852	0.5037	0.6685	0.6111	0.4815	0.4759
WordSynonyms	0.4279	0.4259	0.4122	0.4108	0.4556	0.4426
Worms	0.5688	0.5195	0.6052	0.6143	0.5805	0.5883
WormsTwoClass	0.7052	0.6610	0.7065	0.7403	0.6948	0.7065
Yoga	0.7544	0.7403	0.6602	0.7361	0.7429	0.7716

Table 9: The accuracy of SVM when training on individual windows

Model	SVM_Window_1	SVM_Window_2	SVM_Window_3	SVM_Window_4	SVM_Window_5	SVM_Window_6
50Words	0.4708	0.4738	0.4277	0.4152	0.4587	0.4648
Adiac	0.0348	0.0414	0.0348	0.0345	0.0332	0.0322
ArrowHead	0.2817	0.3640	0.2497	0.2760	0.1989	0.2577
Beef	1.0000	1.0000	0.9333	1.0000	1.0000	0.6333
BeetleFly	0.9900	1.0000	0.9700	0.9700	1.0000	1.0000
BirdChicken	0.8800	1.0000	1.0000	1.0000	0.9550	1.0000
Car	0.2033	0.1767	0.1733	0.1867	0.1850	0.1850
CBF	0.3546	0.4883	0.4962	0.2404	0.4952	0.4012
ChlorineConcentration	0.4767	0.4734	0.4597	0.4685	0.4643	0.4640
CinCECGTorso	0.2598	0.3001	0.2034	0.2770	0.2486	0.2495
Coffee	0.9000	0.7893	0.9393	0.9393	0.9643	0.7964
Computers	1.0000	1.0000	0.8172	0.8832	0.9320	1.0000
CricketX	0.0810	0.0556	0.0782	0.0646	0.0772	0.0838
CricketY	0.0810	0.0818	0.0703	0.0890	0.0800	0.0764
CricketZ	0.0841	0.0769	0.0918	0.0841	0.0813	0.0723
DiatomSizeReduction	0.3729	0.3647	0.3124	0.2533	0.3039	0.3366
DistalPhalanxOutlineAgeGroup	0.5719	0.5698	0.5957	0.7014	0.5381	0.5957
DistalPhalanxOutlineCorrect	0.6399	0.6047	0.6652	0.6971	0.5482	0.5913
DistalPhalanxTW	0.4820	0.5719	0.5065	0.6360	0.6043	0.6007
Earthquakes	0.7424	0.7410	0.7439	0.7453	0.7403	0.7388
ECG200	0.8190	0.8540	0.8150	0.7790	0.7200	0.7400
ECG5000	0.9286	0.9033	0.8040	0.8235	0.9249	0.9320
ECGFiveDays	0.6632	0.6619	0.8676	0.7672	0.7050	0.9034
FaceAll	0.6304	0.5746	0.5769	0.4570	0.4442	0.4002
FaceFour	0.4750	0.5682	0.6830	0.6886	0.4114	0.3182
FacesUCR	0.4201	0.5170	0.5141	0.6624	0.5407	0.5437
Fish	0.5720	0.7966	0.7423	0.7394	0.5886	0.3549
FordA	0.7004	0.6873	0.7365	0.6984	0.7024	0.6982
FordB	0.5763	0.5642	0.5737	0.5995	0.5727	0.5838
GunPoint	0.7160	0.9600	0.7273	0.8040	0.8347	0.8733
Ham	0.6352	0.5190	0.5619	0.5362	0.5981	0.4571
HandOutlines	0.7184	0.8232	0.7478	0.7146	0.7386	0.6335
Haptics	0.3429	0.4010	0.3828	0.3458	0.3873	0.3766
Herring	0.6016	0.5781	0.5609	0.5578	0.5719	0.5547
InlineSkate	0.3953	0.2533	0.2638	0.2836	0.2827	0.3978
InsectWingbeatSound	0.4399	0.4021	0.4052	0.3266	0.3095	0.2644
ItalyPowerDemand	0.6279	0.7944	0.8029	0.8047	0.9376	0.9322
LargeKitchenAppliances	0.5189	0.5021	0.6264	0.5640	0.5563	0.6120
Lightning2	0.6033	0.6213	0.7246	0.6393	0.6902	0.6377
Lightning7	0.3918	0.4027	0.4411	0.4671	0.6712	0.4740
Mallat	0.4956	0.6206	0.4333	0.5373	0.6944	0.6216
Meat	0.8750	0.8933	0.9983	0.8433	0.8783	0.8333
MedicalImages	0.6789	0.5276	0.5536	0.5172	0.5338	0.5639
MiddlePhalanxOutlineAgeGroup	0.3987	0.3669	0.3669	0.5318	0.4545	0.4032
MiddlePhalanxOutlineCorrect	0.4918	0.4708	0.5227	0.6168	0.4948	0.5320
MiddlePhalanxTW	0.4864	0.4760	0.5565	0.5597	0.5162	0.5292
MoteStrain	0.7738	0.8213	0.7577	0.7827	0.8147	0.6998
NonInvasiveFetalECGThorax1	0.7812	0.4126	0.4687	0.3384	0.4824	0.6038
NonInvasiveFetalECGThorax2	0.8419	0.4096	0.5115	0.3733	0.5253	0.7317
OliveOil	0.7067	0.8733	0.6733	0.9000	0.8967	0.7667
OSULeaf	0.6281	0.5657	0.5723	0.5463	0.5802	0.6570
PhalangesOutlinesCorrect	0.6414	0.6076	0.6824	0.7174	0.5988	0.5851
Phoneme	0.1439	0.1598	0.1626	0.1777	0.1543	0.1362
RefrigerationDevices	0.5032	0.5333	0.4237	0.4595	0.4403	0.4619
ScreenType	0.3395	0.3920	0.3299	0.3947	0.4765	0.4373
ShakeGestureWiimoteZ	0.5600	0.3280	0.3440	0.1840	0.1000	0.1000
ShapeletSim	0.5372	0.6106	0.5139	0.4806	0.5722	0.5150
ShapesAll	0.6367	0.6467	0.5817	0.6157	0.6533	0.6633
SmallKitchenAppliances	0.7429	0.6853	0.6787	0.6653	0.6909	0.6483
SonyAIBORobotSurface1	0.7255	0.7233	0.4735	0.6805	0.6556	0.6338
SonyAIBORobotSurface2	0.7487	0.8612	0.7470	0.7031	0.8135	0.7933
StarLightCurves	0.9492	0.9500	0.9170	0.9381	0.9240	0.9345
Strawberry	0.8568	0.9459	0.9119	0.9459	0.8192	0.8595
SwedishLeaf	0.7931	0.6930	0.7552	0.7664	0.7320	0.7645
Symbols	0.6030	0.8141	0.6990	0.8030	0.7397	0.7071
SyntheticControl	0.7920	0.7253	0.7407	0.7803	0.7183	0.7207
ToeSegmentation1	0.5737	0.6548	0.6180	0.6711	0.6039	0.6009
ToeSegmentation2	0.7677	0.5823	0.6923	0.7115	0.6531	0.6385
Trace	0.5350	0.6760	0.5700	0.6890	0.7170	0.3930
TwoLeadECG	0.6672	0.8306	0.9374	0.7199	0.6536	0.5890
TwoPatterns	0.3331	0.3712	0.3844	0.4045	0.5071	0.4035
UWaveGestureLibraryAll	0.7211	0.7467	0.6552	0.6774	0.6879	0.5911
UWaveGestureLibraryX	0.5088	0.6390	0.5861	0.5690	0.6056	0.5796
UWaveGestureLibraryY	0.4736	0.5628	0.5281	0.5251	0.5088	0.5257
UWaveGestureLibraryZ	0.5017	0.5948	0.5486	0.5204	0.5161	0.4902
Wafer	0.9933	0.9901	0.9640	0.9661	0.9852	0.9916
Wine	0.6852	0.5037	0.6685	0.6111	0.4815	0.4759
WordSynonyms	0.4279	0.4259	0.4122	0.4108	0.4556	0.4426
Worms	0.5688	0.5195	0.6052	0.6143	0.5805	0.5883
WormsTwoClass	0.7052	0.6610	0.7065	0.7403	0.6948	0.7065
Yoga	0.7544	0.7403	0.6602	0.7361	0.7429	0.7716